

RESEARCH PAPER



Development of terphenyl-2-methyloxazol-5(4H)-one derivatives as selective reversible MAGL inhibitors

Carlotta Granchi^a , Isabella Caligiuri^b, Eleonora Bertelli^a, Giulio Poli^a, Flavio Rizzolio^c, Marco Macchia^a, Adriano Martinelli^a, Filippo Minutolo^a  and Tiziano Tuccinardi^{a,d} 

^aDepartment of Pharmacy, University of Pisa, Pisa, Italy; ^bUnit of Pathology, Department of Molecular Biology and Translational Research, National Cancer Institute and Center for Molecular Biomedicine, Aviano, Pordenone, Italy; ^cDepartment of Molecular Sciences and Nanosystems, Ca' Foscari Università di Venezia, Venezia-Mestre, Italy; ^dSbarro Institute for Cancer Research and Molecular Medicine, Center for Biotechnology, College of Science and Technology, Temple University, Philadelphia, PA, USA

ABSTRACT

Monoacylglycerol lipase is a serine hydrolase that plays a major role in the degradation of the endocannabinoid neurotransmitter 2-arachidonoylglycerol. A wide number of MAGL inhibitors are reported in literature; however, many of them are characterised by an irreversible mechanism of action and this behavior determines an unwanted chronic MAGL inactivation, which acquires a functional antagonism of the endocannabinoid system. The possible use of reversible MAGL inhibitors has only recently been explored, due to the lack of known compounds possessing efficient reversible inhibitory activities. In this work, we report a new series of terphenyl-2-methyloxazol-5(4H)-one derivatives characterised by a reversible MAGL-inhibition mechanism. Among them, compound **20b** showed to be a potent MAGL reversible inhibitor (IC₅₀ = 348 nM) with a good MAGL/FAAH selectivity. Furthermore, this compound showed antiproliferative activities against two different cancer cell lines that overexpress MAGL.

ARTICLE HISTORY

Received 28 July 2017
Revised 23 August 2017
Accepted 23 August 2017

KEYWORDS



Monoacylglycerol lipase inhibitors; endocannabinoids; docking; molecular dynamic simulations

Introduction

Endocannabinoids are lipid transmitters that act as endogenous ligands of the CB₁ and CB₂ cannabinoid receptors. The endogenous ligands 2-arachidonoylglycerol (2-AG) and *N*-arachidonoyl ethanolamine (AEA) are considered as the two major endocannabinoids and modulate multiple physiological processes including pain, inflammation, appetite, memory and emotion¹. Their signaling activity is terminated by enzymatic hydrolysis, which is mainly mediated by serine hydrolase monoacylglycerol lipase (MAGL) and fatty acid amide hydrolase (FAAH), respectively². Because of its key role in 2-AG catabolism, selective inactivation of MAGL represents an interesting approach for obtaining the desirable effects of indirect cannabinoid receptors activation. MAGL inhibition in the periphery produces CB₁-dependent antinociceptive effects in mouse models of noxious chemical, inflammatory, thermal and neuropathic pain³. Pharmacological and genetic blockades of MAGL exhibit anti-inflammatory effects in the brain and neuroprotective effects in mouse models of Parkinson's and Alzheimer's disease⁴. Other studies suggest that MAGL inhibition produces anti-anxiety responses⁵ and could be useful for modulating drug dependence of opiates⁶. Finally, MAGL is upregulated in aggressive cancer cells and primary tumors and its inhibition in aggressive breast, ovarian, and melanoma cancer cells impairs cell migration, invasiveness, and tumorigenicity⁷. Over the past 10 years, great efforts have been done for identifying novel MAGL inhibitors^{8–13}; however, almost all the reported compounds are characterised by an irreversible MAGL-inhibition mechanism². Among this wide class of MAGL inhibitors, **JZL184**¹¹ and **CAY10499**⁸ (Figure 1) are the two main compounds that are used as reference inhibitors for most of

the cellular and animal experiments in which MAGL is studied. However, as reported by Scholsburg et al.¹⁴, the repeated administrations in mice of an irreversible MAGL inhibitor produces cross-tolerance to CB₁ agonists. Furthermore, chronic MAGL blockade causes impaired endocannabinoid-dependent synaptic plasticity, physical dependence and desensitised brain CB₁ receptors¹⁴. Considering all these negative effects associated to the irreversible MAGL inhibition, the need to discover selective and reversible MAGL inhibitors constitutes a challenging opportunity to target MAGL with minimal occurrence of unwanted side effects. To our knowledge, only few compounds described as good reversible MAGL inhibitors have so far been reported in literature. In 2014, a reversible MAGL inhibitor (compound **c21**, Figure 1) was tested *in vivo* using the EAE (experimental allergic encephalomyelitis) mouse model and the ligand ameliorated the clinical progression of the multiple sclerosis mouse model. Very importantly, the therapeutic effects were not accompanied by catalepsy or other motor impairments which have been instead observed after the administration of irreversible MAGL inhibitors¹⁵. Finally, in 2016, Tuccinardi et al.¹⁶ reported a novel class of benzoylpiperidine derivatives as potent and selective MAGL reversible inhibitors possessing antiproliferative activity against ovarian cancer cell lines (Figure 1, compound **17b**)¹⁷.

Very recently, the same authors developed a class of biphenyl 2-methyloxazol-5(4H)-one compounds of general structure **A** (Figure 2) that inhibits MAGL reversibly and selectively. Modeling studies revealed that the pharmacophoric portions are both the 2-methyloxazol-5(4H)-one ring, interacting with the catalytic S122 of the enzyme, and the peripheral phenyl ring, which

CONTACT Tiziano Tuccinardi  tiziano.tuccinardi@unipi.it  Department of Pharmacy, University of Pisa, Via Bonanno 6, 56126 Pisa, Italy

© 2017 The Author(s). Published by Informa UK Limited, trading as Taylor & Francis Group.

This is an Open Access article distributed under the terms of the Creative Commons Attribution License (<http://creativecommons.org/licenses/by/4.0/>), which permits unrestricted use, distribution, and reproduction in any medium, provided the original work is properly cited.

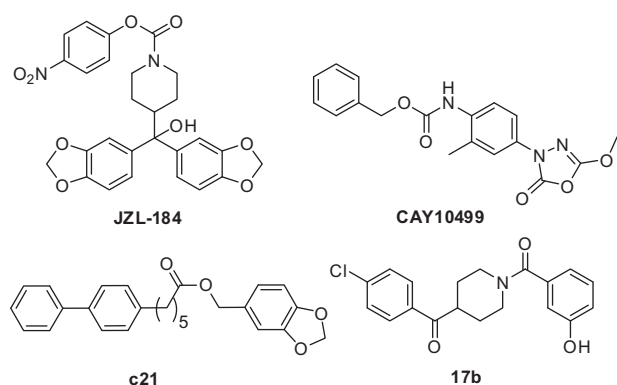


Figure 1. Structures of some of the most relevant MAGL inhibitors.

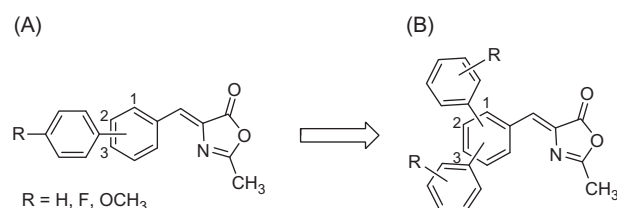


Figure 2. Structural evolution of methylenoxazol-5(4H)-one scaffold: previously developed biphenyl 2-methyloxazol-5(4H)-one compounds (A) and newly synthesised terphenyl-2-methyloxazol-5(4H)-one derivatives (B).

nically fits into a lipophilic cavity of the protein¹⁸. On the basis of these results, and considering the wide available space within the MAGL lipophilic cavity, we decided to add a second aromatic portion, in order to adequately fill this region, while maintaining the same central scaffold of the previous series of compounds (general structure **B**, Figure 2). Therefore, we initially designed and synthesised terphenyl-2-methyloxazol-5(4H)-one derivatives displaying all the possible combinations of substitution positions on the central phenyl ring by inserting unsubstituted phenyl rings. In a second time, after a preliminary evaluation, the best obtained regioisomeric compound in terms of inhibitory enzymatic activity was selected for further fine chemical modifications and, therefore, variously substituted phenyl rings were introduced in the selected positions to determine which kind of group was most suitable to improve MAGL inhibitory potency and enzyme selectivity properties.

Material and methods

Chemistry

Commercially available chemicals were purchased from Sigma-Aldrich (St. Louis, MO, USA) or Alfa Aesar-Thermo Fisher Scientific (Karlsruhe, Germany) and used without further purification. **JZL-184** and **CAY10499** were purchased from Cayman Chemical. NMR spectra were obtained with a Bruker Avance III 400 MHz spectrometer. Chemical shifts (δ) are reported in parts per million downfield from tetramethylsilane and referenced from solvent references. HPLC analysis: all target compounds (i.e. assessed in biological assays) were $\geq 94\%$ pure by HPLC, confirmed via UV detection ($\lambda = 310$ nm). Analytical reversed-phase HPLC was conducted using a Kinetex EVO C18 column (5 μ m, 150 \times 4.6 mm, Phenomenex, Inc.); eluent A, water; eluent B, CH₃CN; after 3 min at 25% B, a gradient was formed from 25 to 85% of B in 4 min and held at 85% of B for 8 min; flow rate was 1 ml/min. Chromatographic

separations were performed on silica gel columns by flash chromatography (Kieselgel 60, 0.040–0.063 mm; Merck). Reactions were followed by thin-layer chromatography (TLC) on Aldrich aluminum silica gel (F254) sheets that were visualised under a UV lamp. Evaporation was performed *in vacuo* (rotating evaporator). Sodium sulfate was always used as the drying agent. Elemental analysis has been used to determine the purity of target compounds. Analytical results are within $\pm 0.40\%$ of the theoretical values.

General procedure for the formation of terphenyl derivatives 6, 12, 14 and 19a–h

A solution of Pd(OAc)₂ (0.06 eq) and triphenylphosphine (0.30 eq) in absolute ethanol (6 ml/2.7 mmol halogenated derivative) and toluene (6 ml/2.7 mmol halogenated derivative) was stirred at room temperature (RT) under nitrogen for 10 min. After that period, commercially available dibromo- or dichloro-substituted aldehydes **2**, **10** or **11** (1 eq), 2 M aqueous Na₂CO₃ (6 ml/2.7 mmol halogenated derivative), and opportunely substituted phenylboronic acid (3.2 eq) were sequentially added. The resulting mixture was heated at 100 °C in a sealed vial under nitrogen for 24 h. After being cooled to RT, it was checked by TLC and if starting material was still present or it was visible the presence of two close spots (probable mono- and di-substitution products), it was added Pd(OAc)₂ (0.03 eq), triphenylphosphine (0.15 eq) and phenylboronic acid (1.6 eq). The mixture was heated again at 100 °C for further 24 h. Finally, the mixture was cooled to RT, diluted with water and extracted with EtOAc. The combined organic phase was dried and concentrated. The crude product was purified by flash chromatography using the indicated eluent and pure fractions containing the desired compound were evaporated to dryness affording the desired product.

(1,1':3',1''-Terphenyl)-4'-carbaldehyde (6)

Yellow crystalline solid, yield: 94% (277.4 mg) from **2** and phenylboronic acid. $R_f = 0.11$ (*n*-hexane/EtOAc 98:2). ¹H-NMR (CDCl₃, 400 MHz) δ (ppm): 7.39–7.53 (m, 8H), 7.65–7.70 (m, 3H), 7.73 (dd, 1H, $J = 8.2, 1.0$ Hz), 8.12 (d, 1H, $J = 8.0$ Hz), 10.02 (s, 1H).

(1,1':3',1''-Terphenyl)-5'-carbaldehyde (12)

White solid, yield: 93% (274.0 mg) from **10** and phenylboronic acid. $R_f = 0.08$ (*n*-hexane/EtOAc 98:2). ¹H-NMR (CDCl₃, 400 MHz) δ (ppm): 7.43 (tt, 2H, $J = 7.4, 1.7$ Hz), 7.48–7.53 (m, 4H), 7.67–7.71 (m, 4H), 8.06–8.10 (m, 3H), 10.16 (s, 1H).

(1,1':4',1''-Terphenyl)-2'-carbaldehyde (14)

White solid, yield: 80% (236.0 mg) from **11** and phenylboronic acid. $R_f = 0.17$ (*n*-hexane/EtOAc 98:2). ¹H-NMR (CDCl₃, 400 MHz) δ (ppm): 7.38–7.57 (m, 9H), 7.67–7.71 (m, 2H), 7.89 (dd, 1H, $J = 8.0, 2.1$ Hz), 8.28 (d, 1H, $J = 2.0$ Hz), 10.05 (s, 1H).

4,4'-Difluoro-(1,1':4',1''-terphenyl)-2'-carbaldehyde (19a)

White solid, yield: 97% (325.5 mg) from **11** and 4-fluorophenylboronic acid. $R_f = 0.18$ (*n*-hexane/EtOAc 98:2). ¹H-NMR (CDCl₃, 400 MHz) δ (ppm): 7.14–7.22 (m, 4H), 7.39 (double AA'XX', 2H, ⁴J_{HF-m} = 5.3 Hz, $J_{AX} = 8.8$ Hz, $J_{AA'/XX'} = 2.5$ Hz), 7.50 (d, 1H, $J = 7.9$ Hz), 7.64 (double AA'XX', 2H, ⁴J_{HF-m} = 5.2 Hz, $J_{AX} = 8.8$ Hz, $J_{AA'/XX'} = 2.6$ Hz), 7.83 (dd, 1H, $J = 8.0, 2.1$ Hz), 8.20 (d, 1H, $J = 2.0$ Hz), 10.02 (s, 1H).

4,4''-Dimethoxy-(1,1':4',1''-terphenyl)-2'-carbaldehyde (19b)

White solid, yield: 99% (363.5 mg) from **11** and 4-methoxyphenylboronic acid. $R_f=0.25$ (*n*-hexane/EtOAc 9:1). $^1\text{H-NMR}$ (CDCl_3 , 400 MHz) δ (ppm): 3.87 (s, 3H), 3.89 (s, 3H), 6.99–7.05 (m, 4H), 7.35 (AA'XX', 2H, $J_{\text{AX}}=8.8$ Hz, $J_{\text{AA'}/\text{XX'}}=2.1$ Hz), 7.49 (d, 1H, $J=8.0$ Hz), 7.62 (AA'XX', 2H, $J_{\text{AX}}=8.9$ Hz, $J_{\text{AA'}/\text{XX'}}=2.2$ Hz), 7.82 (dd, 1H, $J=8.0$, 2.1 Hz), 8.20 (d, 1H, $J=2.0$ Hz), 10.05 (s, 1H).

4,4''-Bis(trifluoromethoxy)-(1,1':4',1''-terphenyl)-2'-carbaldehyde (19c)

Colorless oil, yield: 89% (432.1 mg) from **11** and 4-trifluoromethoxyphenylboronic acid. $R_f=0.13$ (*n*-hexane/EtOAc 99:1). $^1\text{H-NMR}$ (CDCl_3 , 400 MHz) δ (ppm): 7.32–7.38 (m, 4H), 7.46 (AA'XX', 2H, $J_{\text{AX}}=8.8$ Hz, $J_{\text{AA'}/\text{XX'}}=2.4$ Hz), 7.52 (d, 1H, $J=8.0$ Hz), 7.69 (AA'XX', 2H, $J_{\text{AX}}=8.9$ Hz, $J_{\text{AA'}/\text{XX'}}=2.5$ Hz), 7.86 (dd, 1H, $J=8.0$, 2.2 Hz), 8.23 (d, 1H, $J=1.8$ Hz), 10.03 (s, 1H).

4,4''-Bis(trifluoromethyl)-(1,1':4',1''-terphenyl)-2'-carbaldehyde (19d)

White solid, yield: 95% (424.8 mg) from **11** and 4-trifluoromethylphenylboronic acid. $R_f=0.15$ (*n*-hexane/EtOAc 99:1). $^1\text{H-NMR}$ (CDCl_3 , 400 MHz) δ (ppm): 7.54–7.59 (m, 3H), 7.74–7.81 (m, 6H), 7.92 (dd, 1H, $J=8.0$, 2.1 Hz), 8.30 (d, 1H, $J=1.8$ Hz), 10.03 (s, 1H).

3,3''-Difluoro-(1,1':4',1''-terphenyl)-2'-carbaldehyde (19e)

White solid, yield: 94% (316.0 mg) from **11** and 3-fluorophenylboronic acid. $R_f=0.10$ (*n*-hexane/EtOAc 98:2). $^1\text{H-NMR}$ (CDCl_3 , 400 MHz) δ (ppm): 7.07–7.14 (m, 1H), 7.14–7.21 (m, 3H), 7.35–7.40 (m, 1H), 7.42–7.50 (m, 3H), 7.53 (d, 1H, $J=8.0$ Hz), 7.87 (dd, 1H, $J=8.0$, 2.1 Hz), 8.25 (d, 1H, $J=2.0$ Hz), 10.04 (s, 1H).

2,5-Bis[benzo(d)(1,3)dioxol-5-yl]benzaldehyde (19f)

Dark yellow solid, yield: 75% (295.6 mg) from **11** and 3,4-(methylenedioxy)phenylboronic acid. $R_f=0.18$ (*n*-hexane/EtOAc 9:1). $^1\text{H-NMR}$ (CDCl_3 , 400 MHz) δ (ppm): 6.03 (s, 2H), 6.06 (s, 2H), 6.83 (dd, 1H, $J=7.8$, 1.9 Hz), 6.89–6.94 (m, 3H), 7.12–7.16 (m, 2H), 7.47 (d, 1H, $J=8.0$ Hz), 7.77 (dd, 1H, $J=8.0$, 2.1 Hz), 8.15 (d, 1H, $J=2.0$ Hz), 10.05 (s, 1H).

3,3''-Difluoro-4,4''-dimethoxy-(1,1':4',1''-terphenyl)-2'-carbaldehyde (19g)

Pearly white solid, yield: 82% (329.5 mg) from **11** and 3-fluoro-4-methoxyphenylboronic acid. $R_f=0.13$ (*n*-hexane/EtOAc 9:1). $^1\text{H-NMR}$ (CDCl_3 , 400 MHz) δ (ppm): 3.96 (s, 3H), 3.97 (s, 3H), 7.04–7.12 (m, 3H), 7.19 (dd, 1H, $J=11.6$, 2.0 Hz), 7.38–7.44 (m, 2H), 7.48 (d, 1H, $J=8.0$ Hz), 7.80 (dd, 1H, $J=8.0$, 2.1 Hz), 8.18 (d, 1H, $J=2.0$ Hz), 10.05 (s, 1H).

4,4''-Dichloro-(1,1':4',1''-terphenyl)-2'-carbaldehyde (19h)

White solid, yield: 61% (143.0 mg) from **11** and 4-chlorophenylboronic acid. $R_f=0.40$ (*n*-hexane/EtOAc 98:2). $^1\text{H-NMR}$ (CDCl_3 , 400 MHz) δ (ppm): 7.36 (AA'XX', 2H, $J_{\text{AX}}=8.6$ Hz, $J_{\text{AA'}/\text{XX'}}=2.3$ Hz), 7.44–7.52 (m, 5H), 7.61 (AA'XX', 2H, $J_{\text{AX}}=8.7$ Hz, $J_{\text{AA'}/\text{XX'}}=2.3$ Hz), 7.85 (dd, 1H, $J=8.0$, 2.1 Hz), 8.22 (d, 1H, $J=2.1$ Hz), 10.03 (s, 1H).

Procedure for the synthesis of (1,1':2',1''-terphenyl)-4'-carbaldehyde (4)

3,4-Dichlorobenzaldehyde **1** (500 mg, 2.86 mmol, 1 eq) was placed in a vial together with phenylboronic acid (1.39 g, 11.4 mmol),

potassium phosphate (2.67 g, 12.6 mmol), $\text{Pd}(\text{OAc})_2$ (57.8 mg, 0.0858 mmol), tetrabutylammonium bromide (TBAB) (14.3 g, 44.3 mmol) and water (6.4 ml). The vial was sealed and heated under stirring at 125 °C for 48 h. The reaction mixture was cooled to RT and then diluted with water. The water phase was acidified with 1 N aqueous HCl and repeatedly extracted with EtOAc. The combined organic phase was washed with brine, dried over anhydrous sodium sulfate and evaporated to afford a crude residue that was purified by column chromatography over silica gel using *n*-hexane/EtOAc 98:2 ($R_f=0.16$) as the eluent, to give pure **4** as a yellow oily compound (157.9 mg, 21% yield). $^1\text{H-NMR}$ (DMSO-d_6 , 400 MHz) δ (ppm): 7.14–7.20 (m, 4H), 7.25–7.32 (m, 6H), 7.65 (d, 1H, $J=8.0$ Hz), 7.94 (d, 1H, $J=1.2$ Hz), 7.98 (dd, 1H, $J=7.6$, 1.6 Hz), 10.11 (s, 1H).

Procedure for the synthesis of (1,1':2',1''-terphenyl)-3'-carbaldehyde (8)

A solution of $\text{Pd}(\text{OAc})_2$ (0.06 eq) and triphenylphosphine (0.30 eq) in absolute ethanol (6 ml/2.7 mmol halogenated derivative) and toluene (6 ml/2.7 mmol halogenated derivative) was stirred at RT under nitrogen for 10 min. After that period, commercially available 2,3-dichlorobenzaldehyde **3** (300 mg, 1.71 mmol, 1 eq), 2 M aqueous Na_2CO_3 (6 ml/2.7 mmol halogenated derivative), and phenylboronic acid (3.2 eq) were sequentially added. The resulting mixture was heated at 100 °C in a sealed vial under nitrogen for 24 h. After being cooled to RT, the mixture was diluted with water and extracted with EtOAc. The combined organic phase was dried and concentrated. Since $^1\text{H-NMR}$ analysis revealed the formation of a mono-substitution product, the crude (320 mg) was dissolved in anhydrous dioxane (3.7 ml) and treated, under nitrogen, with cesium carbonate (1.7 eq), phenylboronic acid (1.6 eq), $\text{Pd}_2(\text{dba})_3$ (0.032 eq), and a 20% solution of tricyclohexylphosphine in toluene (0.08 eq). The reaction was heated at 100 °C in a sealed vial overnight. The reaction mixture was then cooled to RT, diluted with EtOAc, and filtered through a Celite pad. The organic filtrate was concentrated under vacuum, and the crude product was purified by flash chromatography (*n*-hexane/EtOAc 99:1, $R_f=0.08$) to yield pure **8** as a white solid (244.3 mg, 55% total yield over two steps). $^1\text{H-NMR}$ (CDCl_3 , 400 MHz) δ (ppm): 7.03–7.07 (m, 2H), 7.08–7.13 (m, 2H), 7.15–7.20 (m, 3H), 7.23–7.29 (m, 3H), 7.56 (t, 1H, $J=7.7$ Hz), 7.65 (dd, 1H, $J=7.6$, 1.5 Hz), 8.04 (dd, 1H, $J=7.8$, 1.5 Hz), 9.81 (s, 1H).

Procedure for the synthesis of (1,1':3',1''-terphenyl)-2'-carbaldehyde (17)

2,6-Dichlorobenzaldehyde **16** (500 mg, 2.86 mmol, 1 eq) was dissolved in anhydrous dioxane (7.2 ml) and treated, under nitrogen, with cesium carbonate (3.4 eq), phenylboronic acid (3.2 eq), $\text{Pd}_2(\text{dba})_3$ (0.064 eq), and a 20% solution of tricyclohexylphosphine in toluene (0.16 eq). The reaction was heated at 100 °C in a sealed vial overnight. After being cooled to RT, it was added $\text{Pd}_2(\text{dba})_3$ (0.032 eq), tricyclohexylphosphine (0.08 eq) and phenylboronic acid (1.6 eq). The mixture was heated again at 100 °C for further 24 h. The reaction mixture was then cooled to RT, diluted with EtOAc, and filtered through a Celite pad. The organic filtrate was concentrated under vacuum, and the crude product was purified by flash chromatography (*n*-hexane/EtOAc 98:2, $R_f=0.13$) to yield pure **17** as a crystalline yellow solid (685 mg, 93% yield). $^1\text{H-NMR}$ (CDCl_3 , 400 MHz) δ (ppm): 7.33–7.47 (m, 12H), 7.60 (dd, 1H, $J=7.9$, 7.4 Hz), 9.96 (s, 1H).

General procedure for the preparation of the 2-methyloxazol-5(4H)-one derivatives 5, 7, 9, 13, 15

A mixture of diphenyl-substituted benzaldehydes **4**, **6**, **8**, **12** or **14** (1 eq), *N*-acetylglycine (1 eq) and sodium acetate (1 eq) in acetic

anhydride (5 ml/5 mmol aldehyde) was stirred at reflux for 5 h and then warmed to RT. The reaction was quenched with water and extracted with AcOEt. The organic layer was washed sequentially with water and saturated brine, dried over Na₂SO₄ and the solvent was removed under reduced pressure. The residue was purified with a flash column chromatography using the indicated eluent and pure fractions containing the desired compound were evaporated to dryness affording the desired product.

(Z)-4-[(1,1':2',1''-Terphenyl)-4'-ylmethylene]-2-methyloxazol-5(4H)-one (5)

Yellow solid, yield: 23% (44.4 mg) from **4**. *R_f*=0.21 (*n*-hexane/EtOAc 95:5). ¹H-NMR (CDCl₃, 400 MHz) δ (ppm): 2.41 (s, 3H), 7.12–7.18 (m, 4H), 7.20–7.27 (m, 7H), 7.52 (d, 1H, *J*=8.0 Hz), 8.07 (d, 1H, *J*=1.8 Hz), 8.19 (dd, 1H, *J*=8.2, 1.7 Hz). ¹³C-NMR (CDCl₃, 100 MHz) δ (ppm): 15.86, 127.01, 127.22, 128.16 (2 C), 128.19 (2 C), 129.86 (2 C), 129.99 (2 C), 131.09, 131.14, 131.36, 132.54, 132.96, 134.56, 140.75, 140.86, 141.34, 143.50, 166.29, 167.98. HPLC analysis: retention time = 11.207 min; peak area, 95%. Elemental analysis for C₂₃H₁₇NO₂ calculated: % C, 81.40; % H, 5.05; % N, 4.13; found: % C, 81.10; % H, 5.03; % N, 4.12.

(Z)-4-[(1,1':3',1''-Terphenyl)-4'-ylmethylene]-2-methyloxazol-5(4H)-one (7)

Yellow solid, yield: 11% (55.2 mg) from **6**. *R_f*=0.13 (*n*-hexane/EtOAc 95:5). ¹H-NMR (CDCl₃, 400 MHz) δ (ppm): 2.43 (s, 3H), 7.24 (s, 1H), 7.35–7.50 (m, 8H), 7.63–7.69 (m, 3H), 7.72 (dd, 1H, *J*=8.3, 1.9 Hz), 8.79 (d, 1H, *J*=8.3 Hz). ¹³C-NMR (CDCl₃, 100 MHz) δ (ppm): 15.89, 126.48, 127.29, 127.35, 128.19, 128.30, 128.62, 128.69 (2 C), 129.05, 129.11 (2 C), 129.15, 130.06, 130.09, 132.70, 132.71, 139.95, 140.09, 143.40, 145.72, 166.25, 167.75. HPLC analysis: retention time = 11.349 min; peak area, 96%. Elemental analysis for C₂₃H₁₇NO₂ calculated: % C, 81.40; % H, 5.05; % N, 4.13; found: % C, 81.32; % H, 5.04; % N, 4.12.

(Z)-4-[(1,1':2',1''-Terphenyl)-3'-ylmethylene]-2-methyloxazol-5(4H)-one (9)

Yellow solid, yield: 13% (39.4 mg) from **8**. *R_f*=0.14 (*n*-hexane/EtOAc 95:5). ¹H-NMR (CDCl₃, 400 MHz) δ (ppm): 2.41 (s, 3H), 6.90–7.05 (m, 5H), 7.12–7.17 (m, 3H), 7.20–7.25 (m, 3H), 7.48 (dd, 1H, *J*=7.6, 1.5 Hz), 7.54 (t, 1H, *J*=7.7 Hz), 8.65 (dd, 1H, *J*=7.8, 1.4 Hz). ¹³C-NMR (CDCl₃, 100 MHz) δ (ppm): 15.86, 126.64, 127.57, 127.81 (3 C), 128.01 (2 C), 129.82 (2 C), 130.97, 131.03, 131.29 (2 C), 132.23, 132.74, 132.87, 138.12, 141.21, 142.40, 143.29, 166.41, 167.56. HPLC analysis: retention time = 10.983 min; peak area, 94%. Elemental analysis for C₂₃H₁₇NO₂ calculated: % C, 81.40; % H, 5.05; % N, 4.13; found: % C, 81.07; % H, 5.03; % N, 4.11.

(Z)-4-[(1,1':3',1''-Terphenyl)-5'-ylmethylene]-2-methyloxazol-5(4H)-one (13)

Yellow solid, yield: 41% (142.0 mg) from **12**. *R_f*=0.17 (*n*-hexane/EtOAc 95:5). ¹H-NMR (CDCl₃, 400 MHz) δ (ppm): 2.43 (s, 3H), 7.27 (s, 1H), 7.41 (tt, 2H, *J*=7.3, 1.5 Hz), 7.47–7.53 (m, 4H), 7.66–7.70 (m, 4H), 7.86 (t, 1H, *J*=1.7 Hz), 8.30 (d, 2H, *J*=1.6 Hz). ¹³C-NMR (CDCl₃, 100 MHz) δ (ppm): 15.73, 128.06, 128.76, 128.84, 129.89 (11 C), 130.36, 130.58, 134.59, 135.60, 141.13, 143.16, 168.14, 168.21. HPLC analysis: retention time = 11.496 min; peak area, 97%. Elemental analysis for C₂₃H₁₇NO₂ calculated: % C, 81.40; % H, 5.05; % N, 4.13; found: % C, 81.68; % H, 5.06; % N, 4.14.

(Z)-4-[(1,1':4',1''-Terphenyl)-2'-ylmethylene]-2-methyloxazol-5(4H)-one (15)

Yellow solid, yield: 15% (43.0 mg) from **14**. *R_f*=0.18 (*n*-hexane/EtOAc 95:5). ¹H-NMR (CDCl₃, 400 MHz) δ (ppm): 2.42 (s, 3H), 7.11 (s, 1H), 7.41–7.57 (m, 9H), 7.75–7.79 (m, 2H), 7.84 (dd, 1H, *J*=8.0, 2.0 Hz), 9.10 (d, 1H, *J*=2.0 Hz). ¹³C-NMR (CDCl₃, 100 MHz) δ (ppm): 15.74, 127.82 (3 C), 128.67, 128.70, 128.86, 129.44 (2 C), 129.92, 129.97 (2 C), 130.80 (2 C), 131.16, 131.80, 132.19, 134.52, 140.52, 141.24, 144.54, 168.16, 168.23. HPLC analysis: retention time = 11.425 min; peak area, 95%. Elemental analysis for C₂₃H₁₇NO₂ calculated: % C, 81.40; % H, 5.05; % N, 4.13; found: % C, 81.65; % H, 5.06; % N, 4.15.

General procedure for the preparation of the 2-methyloxazol-5(4H)-one derivatives 20a–h

The procedure for the synthesis of these compounds is similar to that used for previous analog final products, with the exception of the used equivalents of *N*-acetylglycine (2 eq) and sodium acetate (2 eq).

(Z)-4-[[4,4''-Difluoro-(1,1':4',1''-terphenyl)-2'-yl]methylene]-2-methyloxazol-5(4H)-one (20a)

Yellow solid, yield: 35% (46.5 mg) from **19a**. *R_f*=0.20 (*n*-hexane/EtOAc 95:5). ¹H-NMR (acetone-d₆, 400 MHz) δ (ppm): 2.43 (s, 3H), 7.06 (s, 1H), 7.28–7.34 (m, 4H), 7.48 (double AA'XX', 2H, 4JHF_m = 5.4 Hz, *J*_{AX} = 8.9 Hz, *J*_{AA'/XX'} = 2.2 Hz), 7.55 (d, 1H, *J*=8.0 Hz), 7.78–7.84 (m, 3H), 9.04 (d, 1H, *J*=1.9 Hz). ¹³C-NMR (acetone-d₆, 100 MHz) δ (ppm): 15.71, 116.25 (d, 2 C, *J*=21.4 Hz), 116.69 (d, 2 C, *J*=21.8 Hz), 128.23, 129.75 (d, 2 C, *J*=8.1 Hz), 129.81, 131.03, 131.86, 132.32, 132.74 (d, 2 C, *J*=8.1 Hz), 134.75, 136.68 (d, *J*=3.5 Hz), 137.27 (d, *J*=3.2 Hz), 140.29, 143.29, 163.60 (d, *J*=234.1 Hz), 163.60 (d, *J*=257.3 Hz), 168.07, 168.42. HPLC analysis: retention time = 11.375 min; peak area, 96%. Elemental analysis for C₂₃H₁₅F₂NO₂ calculated: % C, 73.59; % H, 4.03; % N, 3.73; found: % C, 73.35; % H, 4.01; % N, 3.72.

(Z)-4-[[4,4''-Dimethoxy-(1,1':4',1''-terphenyl)-2'-yl]methylene]-2-methyloxazol-5(4H)-one (20b)

Yellow solid, yield: 19% (23.8 mg) from **19b**. *R_f*=0.15 (*n*-hexane/EtOAc 9:1). ¹H-NMR (acetone-d₆, 400 MHz) δ (ppm): 2.42 (s, 3H), 3.88 (s, 3H), 3.89 (s, 3H), 7.06–7.11 (m, 4H), 7.14 (s, 1H), 7.35 (AA'XX', 2H, *J*_{AX} = 8.8 Hz, *J*_{AA'/XX'} = 2.6 Hz), 7.49 (d, 1H, *J*=7.8 Hz), 7.70 (AA'XX', 2H, *J*_{AX} = 8.9 Hz, *J*_{AA'/XX'} = 2.6 Hz), 7.77 (dd, 1H, *J*=8.1, 2.1 Hz), 9.03 (d, 1H, *J*=2.0 Hz). ¹³C-NMR (acetone-d₆, 100 MHz) δ (ppm): 15.71, 55.60, 55.65, 114.55 (2 C), 114.85, 115.27 (2 C), 115.36, 128.67 (2 C), 128.82, 129.46, 130.62, 131.70, 131.84 (2 C), 131.99, 132.10, 139.79, 140.48, 160.38, 160.51, 166.44, 168.25. HPLC analysis: retention time = 11.155 min; peak area, 95%. Elemental analysis for C₂₅H₂₁NO₄ calculated: % C, 75.17; % H, 5.30; % N, 3.51; found: % C, 74.90; % H, 5.28; % N, 3.50.

(Z)-4-[[4,4''-Bis(trifluoromethoxy)-(1,1':4',1''-terphenyl)-2'-yl]methylene]-2-methyloxazol-5(4H)-one (20c)

Yellow solid, yield: 32% (161.3 mg) from **19c**. *R_f*=0.08 (*n*-hexane/EtOAc 98:2). ¹H-NMR (acetone-d₆, 400 MHz) δ (ppm): 2.43 (s, 3H), 7.06 (s, 1H), 7.48–7.53 (m, 4H), 7.57–7.62 (m, 3H), 7.86–7.90 (m, 1H), 7.91 (AA'XX', 2H, *J*_{AX} = 8.6 Hz, *J*_{AA'/XX'} = 1.9 Hz), 9.09 (d, 1H, *J*=1.8 Hz). ¹³C-NMR (acetone-d₆, 100 MHz) δ (ppm): 15.74, 121.54 (q, 2 C, *J*=256.0 Hz), 121.94, 122.51, 127.87, 129.64 (2 C), 129.97 (2 C), 131.29, 131.99 (2 C), 132.42, 132.64 (2 C), 135.07, 139.52,

140.04, 140.15, 143.19, 149.83, 149.84, 168.00, 168.66. HPLC analysis: retention time = 13.106 min; peak area, 94%. Elemental analysis for $C_{25}H_{15}F_6NO_4$ calculated: % C, 59.18; % H, 2.98; % N, 2.76; found: % C, 59.40; % H, 2.99; % N, 2.77.

(Z)-4-[[4,4'-Bis(trifluoromethyl)-(1,1':4',1''-terphenyl)-2'-yl]methylene]-2-methyloxazol-5(4H)-one (20d)

Yellow solid, yield: 54% (260.3 mg) from **19d**. $R_f = 0.18$ (*n*-hexane/EtOAc 9:1). 1H -NMR (acetone- d_6 , 400 MHz) δ (ppm): 2.44 (s, 3H), 7.04 (s, 1H), 7.65 (d, 1H, $J = 8.0$ Hz), 7.68–7.73 (m, 2H), 7.87–7.93 (m, 4H), 7.96 (dd, 1H, $J = 8.1, 2.0$ Hz), 7.99–8.04 (m, 2H), 9.16 (d, 1H, $J = 2.0$ Hz). ^{13}C -NMR (acetone- d_6 , 100 MHz) δ (ppm): 15.75, 125.36 (q, $J = 271.5$ Hz), 125.45 (q, $J = 271.2$ Hz), 126.37 (q, 2 C, $J = 3.7$ Hz), 126.91 (q, 2 C, $J = 3.9$ Hz), 127.46, 128.60, 130.14, 130.27 (q, $J = 32.3$ Hz), 130.48 (q, $J = 32.3$ Hz), 131.57 (2 C), 132.02, 132.51, 135.34, 140.33, 143.55, 144.41 (q, 2 C, $J = 1.4$ Hz), 144.70 (q, 2 C, $J = 1.4$ Hz), 167.93, 168.87. HPLC analysis: retention time = 12.638 min; peak area, 97%. Elemental analysis for $C_{25}H_{15}F_6NO_2$ calculated: % C, 63.16; % H, 3.18; % N, 2.95; found: % C, 63.38; % H, 3.17; % N, 2.96.

(Z)-4-[[3,3'-Difluoro-(1,1':4',1''-terphenyl)-2'-yl]methylene]-2-methyloxazol-5(4H)-one (20e)

Yellow solid, yield: 45% (89.5 mg) from **19e**. $R_f = 0.20$ (*n*-hexane/EtOAc 95:5). 1H -NMR (acetone- d_6 , 400 MHz) δ (ppm): 2.43 (s, 3H), 7.05 (s, 1H), 7.18–7.30 (m, 4H), 7.48–7.63 (m, 5H), 7.87 (dd, 1H, $J = 8.0, 2.0$ Hz), 9.07 (d, 1H, $J = 2.0$ Hz). ^{13}C -NMR (acetone- d_6 , 100 MHz) δ (ppm): 15.75, 114.48 (d, $J = 22.8$ Hz), 115.44 (d, $J = 21.3$ Hz), 115.70 (d, $J = 21.3$ Hz), 117.47 (d, $J = 22.0$ Hz), 123.80 (d, $J = 2.9$ Hz), 126.95 (d, $J = 2.9$ Hz), 127.83, 129.90, 131.22, 131.35 (d, $J = 8.1$ Hz), 131.88 (d, $J = 9.9$ Hz), 132.34, 135.02, 140.22, 142.73 (d, $J = 7.9$ Hz), 143.29 (d, $J = 7.3$ Hz), 143.45, 143.47, 163.56 (d, $J = 245.7$ Hz), 164.21 (d, $J = 244.3$ Hz), 168.02, 168.63. HPLC analysis: retention time = 11.405 min; peak area, 97%. Elemental analysis for $C_{23}H_{15}F_2NO_2$ calculated: % C, 73.59; % H, 4.03; % N, 3.73; found: % C, 73.40; % H, 4.02; % N, 3.72.

(Z)-4-[[2,5-Bis(benzo[d][1,3]dioxol-5-yl)benzylidene]-2-methyloxazol-5(4H)-one (20f)

Yellow solid, yield: 11% (25.9 mg) from **19f**. $R_f = 0.10$ (*n*-hexane/Et $_2$ O 9:1). 1H -NMR (acetone- d_6 , 400 MHz) δ (ppm): 2.42 (s, 3H), 6.09 (s, 2H), 6.11 (s, 2H), 6.86 (dd, 1H, $J = 8.0, 1.8$ Hz), 6.93 (d, 1H, $J = 1.6$ Hz), 6.97–7.01 (m, 2H), 7.14 (s, 1H), 7.22–7.27 (m, 2H), 7.48 (d, 1H, $J = 8.0$ Hz), 7.74 (dd, 1H, $J = 8.1, 2.1$ Hz), 8.97 (d, 1H, $J = 2.0$ Hz). ^{13}C -NMR (acetone- d_6 , 100 MHz) δ (ppm): 15.73, 66.82, 66.93, 102.39, 102.49, 108.02, 109.04, 109.55, 110.91, 121.47, 124.64, 128.92, 129.63, 130.82, 131.71, 132.22, 134.31, 135.23, 140.74, 143.81, 148.61, 148.93, 149.48, 168.08, 168.22. HPLC analysis: retention time = 10.849 min; peak area, 95%. Elemental analysis for $C_{25}H_{17}NO_6$ calculated: % C, 70.25; % H, 4.01; % N, 3.28; found: % C, 69.98; % H, 3.99; % N, 3.27.

(Z)-4-[[3,3'-Difluoro-4,4'-dimethoxy-(1,1':4',1''-terphenyl)-2'-yl]methylene]-2-methyloxazol-5(4H)-one (20g)

Yellow solid, yield: 12% (49.2 mg) from **19g**. $R_f = 0.13$ (*n*-hexane/EtOAc 85:15). 1H -NMR (acetone- d_6 , 400 MHz) δ (ppm): 2.43 (s, 3H), 3.97 (s, 3H), 3.98 (s, 3H), 7.11 (s, 1H), 7.17 (ddd, 1H, $J = 8.4, 2.2, 1.2$ Hz), 7.23 (dd, 1H, $J = 12.1, 2.1$ Hz), 7.28 (td, 2H, $J = 8.7, 3.5$ Hz), 7.50–7.57 (m, 3H), 7.80 (dd, 1H, $J = 8.1, 2.1$ Hz), 9.01 (d, 1H, $J = 2.0$ Hz). ^{13}C -NMR (acetone- d_6 , 100 MHz) δ (ppm): 15.75, 56.65,

56.69, 115.11 (d, $J = 18.9$ Hz), 115.20, 118.18 (d, $J = 18.1$ Hz), 123.76 (d, $J = 3.0$ Hz), 125.60, 127.18 (d, $J = 3.4$ Hz), 128.48, 129.47, 130.71, 131.82, 132.26, 133.13 (d, $J = 6.6$ Hz), 133.83 (d, $J = 6.3$ Hz), 134.68, 139.71, 142.83, 148.56 (d, $J = 3.6$ Hz), 148.67 (d, $J = 3.2$ Hz), 152.84 (d, $J = 245.8$ Hz), 153.48 (d, $J = 244.7$ Hz), 168.15, 168.32. HPLC analysis: retention time = 11.015 min; peak area, 99%. Elemental analysis for $C_{25}H_{19}F_2NO_4$ calculated: % C, 68.96; % H, 4.40; % N, 3.22; found: % C, 68.97; % H, 4.41; % N, 3.21.

(Z)-4-[[4,4'-Dichloro-(1,1':4',1''-terphenyl)-2'-yl]methylene]-2-methyloxazol-5(4H)-one (20h)

Yellow solid, yield: 7% (18.1 mg) from **19h**. $R_f = 0.18$ (*n*-hexane/EtOAc 95:5). 1H -NMR (acetone- d_6 , 400 MHz) δ (ppm): 2.43 (s, 3H), 7.05 (s, 1H), 7.46 (AA'XX', 2H, $J_{AX} = 8.7$ Hz, $J_{AA'/XX'} = 2.3$ Hz), 7.54–7.59 (m, 5H), 7.79 (AA'XX', 2H, $J_{AX} = 8.8$ Hz, $J_{AA'/XX'} = 2.4$ Hz), 7.85 (dd, 1H, $J = 8.1, 2.0$ Hz), 9.06 (d, 1H, $J = 2.0$ Hz). ^{13}C -NMR (acetone- d_6 , 100 MHz) δ (ppm): 15.73, 127.95, 129.45 (2 C), 129.54 (2 C), 129.80, 130.03 (2 C), 131.10, 131.83, 132.34, 132.43 (2 C), 134.42, 134.65, 134.95, 139.14, 139.61, 140.20, 143.32, 168.01, 168.57. HPLC analysis: retention time = 12.830 min; peak area, 95%. Elemental analysis for $C_{23}H_{15}Cl_2NO_2$ calculated: % C, 67.66; % H, 3.70; % N, 3.43; found: % C, 67.90; % H, 3.71; % N, 3.44.

Biological evaluation

MAGL-inhibition assay

Human recombinant MAGL, and 4-nitrophenylacetate substrate (4-NPA) were from Cayman Chemical. The IC₅₀ values for compounds were generated in 96-well microtiter plates. The MAGL reaction was conducted at RT at a final volume of 200 μ L in 10 mM Tris buffer, pH 7.2, containing 1 mM EDTA. A total of 150 μ L of 4-NPA 133.3 μ M (final concentration = 100 μ M) was added to 10 μ L of DMSO containing the appropriate amount of compound. The reaction was initiated by the addition of 40 μ L of MAGL (11 ng/well) in such a way that the assay was linear over 30 min. The final concentration of the analyzed compounds ranged for **CAY10499** and **JZL-184** from 10 to 0.00001 μ M and for the synthesised compounds from 200 to 0.0128 μ M. After the reaction had proceeded for 30 min, absorbance values were then measured by using a VictorX3 PerkinElmer instrument at 405 nm. Two reactions were also run: one reaction containing no compounds and the second one containing neither inhibitor nor enzyme. IC₅₀ values were derived from experimental data using the Sigmoidal dose–response fitting of GraphPad Prism software as reported earlier¹⁶. To remove possible false positive results, for each compound concentration a blank analysis was carried out, and the final absorbance results were obtained subtracting the absorbance produced by the presence of all the components except MAGL in the same conditions.

MAGL preincubation assay

The MAGL reaction was conducted at RT at a final volume of 200 μ L in 10 mM Tris buffer, pH 7.2, containing 1 mM EDTA. A total of 150 μ L of MAGL (11 ng/well) was added to 10 μ L of DMSO containing the appropriate amount of compound. After 0, 30, and 60 min of incubation time the reaction was initiated by the addition of 40 μ L of 4-NPA 500 μ M. The enzyme activity was then measured according to the procedure described above.

MAGL dilution assay

The enzyme (880 ng in 75 μ L of Tris buffer, pH 7.2) was incubated during 60 min at RT with 5 μ L of compound **20b** (concentration of 10 μ M in the mixture) dissolved in DMSO. The MAGL-inhibitor

mixture was then diluted 40-fold with the buffer. After 15 min of incubation, the reaction was initiated on a 160 μL aliquot by the addition of 40 μL of 4-NPA 500 μM and the enzyme activity was measured according to the procedure described above.

FAAH inhibition assay

The IC_{50} values for compounds were generated in 96-well microtiter plates. The FAAH reaction was conducted at RT at a final volume of 200 μL in 125 mM Tris buffer, pH 9.0, containing 1 mM EDTA. A total of 150 μL of AMC arachidonoyl amide 13.3 μM (final concentration = 10 μM) was added to 10 μL of DMSO containing the appropriate amount of compound. The reaction was initiated by the addition of 40 μL of FAAH (0.9 $\mu\text{g}/\text{well}$) in such a way that the assay was linear over 30 min. After the reaction had proceeded for 30 min, fluorescence values were then measured by using a VictorX3 PerkinElmer instrument at an excitation wavelength of 340 nm and an emission of 460 nm. Two reactions were also run: one reaction containing no compounds and the second one containing neither inhibitor nor enzyme. IC_{50} values were derived from experimental data using the Sigmoidal dose–response fitting of GraphPad Prism software as reported earlier¹⁹. To remove possible false-positive results, for each compound concentration, a blank analysis was carried out, and the final fluorescence results were obtained subtracting the fluorescence produced by the presence of all the components except FAAH in the same conditions.

Cell viability assay

COV318, OVCAR-3 (from ATCC) and hMSC (from AB Cell-Bio) were maintained at 37 °C in a humidified atmosphere containing 5% CO_2 accordingly to the supplier. Normal (1.5×10^4) and tumor (5×10^2) cells were plated in 96-well culture plates. The day after seeding, vehicle or compounds were added at different concentrations to the medium. Compound was added to the cell culture at a concentration ranging from 200 to 0.02 μM . Cell viability was measured after 96 h according to the supplier (Promega, G7571) with a Tecan F200 instrument. IC_{50} values were calculated from logistical dose–response curves. Averages were obtained from three independent experiments, and error bars are standard deviations ($n = 3$).

Molecular modeling

Consensus docking studies

The ligand was built by means of Maestro²⁰ and was then minimised in a water environment (using the Generalised Born/surface area model) by means of Macromodel²¹. It was minimised using the conjugate gradient (CG), the MMFFs force field, and a distance-dependent dielectric constant of 1.0 until they reached a convergence value of 0.05 kcal $\text{\AA}^{-1} \text{mol}^{-1}$. Nine different docking procedures were applied and for each docking calculation only the best scored pose was taken into account²². The ligand was docked in the human MAGL (3JWE²³ PDB code) and the humanised-rat FAAH (3LJ7²⁴ PDB code). The ligand was docked into the two proteins by using the different docking procedures, then the root mean square deviation (RMSD) of each of these docking poses against the remaining docking results was evaluated by using the rms_analysis software of the GOLD suite. The most populated cluster was then considered and subjected to molecular dynamic (MD) simulations.

AUTODOCK 4.2.3

AUTODOCK Tools utilities²⁵ were used in order to identify the torsion angles in the ligand, to add the solvent model and assign the

Gasteiger atomic charges to proteins and ligand. The regions of interest used by AUTODOCK²⁶ were defined by considering the reference ligand as the central group of a grid box of 10 \AA in the x, y, and z directions. A grid spacing of 0.375 \AA and a distance-dependent function of the dielectric constant were used for the energetic map calculations. By using the Lamarckian genetic algorithm, the docked compounds were subjected to 20 runs of the AUTODOCK search using 2,500,000 steps of energy evaluation and the default values of the other parameters.

DOCK 6.7

The molecular surface of the binding site was calculated by means of the MS program²⁷, generating the Connolly surface with a probe with a radius of 1.4 \AA . The points of the surface and the vectors normal to it were used by the Sphgen program in order to build a set of spheres, with radii varying from 1.4 to 4.0 \AA that describe, from a stereoelectronic point of view, the negative image of the site. Spheres within a radius of 10 \AA from the reference ligand were used to represent the site. For each docking calculation, DOCK 6.7 calculated 1000 orientations; of these, the best grid scored was taken into consideration. The ligand charge was calculated using the AM1-BCC method, as implemented in the MOLCHARGE program²⁸.

FRED 3.0

FRED²⁹ requires a set of input conformers for each ligand. The conformers were generated by OMEGA2^{30–32}. The following modifications to the default settings of OMEGA2 were applied: the energy window was set at 50.0, the maximum number of output conformers was set at 10,000, the time limit was set at 1200, and the RMSD value below which two conformations were considered to be similar was set at 0.3 \AA ³³. The region of interest for the docking studies was defined in such a manner that it contained all residues which stayed within 10 \AA from the ligand in the X-ray structures. FRED default parameters were used setting the high dock_resolution.

GLIDE 5.0

The binding site was defined by a rectangular box of 10 \AA in the x, y, and z directions centered on the ligand. The option allowing only the docking of ligands containing a defined range of atoms was deactivated, whereas the GLIDE³⁴ defaults were used for all other parameters. Docking calculations were carried out using the standard precision (SP) method.

GOLD 5.1

The region of interest for the docking studies was defined in such a manner that it contained all residues which stayed within 10 \AA from the ligand in the X-ray structures; the “allow early termination” command was deactivated, while the possibility for the ligand to flip ring corners was activated. For all other parameters, GOLD³⁵ defaults were used and the ligands were subjected to 30 genetic algorithm runs. Three docking analyzes were carried out by using three fitness functions implemented in GOLD, i.e. GoldScore (GS), ChemScore (CS) and Astex Statistical Potential (ASP).

AUTODOCK VINA 1.1

The input files for the ligand and proteins originated from the AUTODOCK Tools utilities for the AUTODOCK calculations were also used for the AUTODOCK VINA³⁶ calculations, including the grid box dimensions. The exhaustiveness parameter was set to 10

and the Energy_range to 1, whereas for all other parameters, AUTODOCK VINA defaults were used.

PLANTS

This docking software uses Ant Colony Optimisation, a state-of-the-art global optimisation algorithm to find minima of a scoring function representing favorable complex structures³⁷. ChemPLP scoring function was employed to score protein–ligand interactions as well as intra-ligands clash terms. Standard settings for all parameters were used for the scoring function as well as the optimisation algorithm (search speed setting: “speed1”). The regions of interest used by PLANTS³⁷ were defined by considering the reference ligand as the central group of a grid box of 10 Å in the x, y, and z directions.

MD simulations

All simulations were performed using AMBER, version 14³⁸. MD simulations were carried out using the ff14SB force field at 300 K. The complex was placed in a rectangular parallelepiped water box. An explicit solvent model for water, TIP3P, was used, and the complexes were solvated with a 20 Å water cap. Chlorine or Sodium ions and were added as counter ions to neutralise the system. Prior to MD simulations, two steps of minimisation were carried out using the same procedure described above. Particle mesh Ewald (PME) electrostatics and periodic boundary conditions were used in the simulation³⁹. The MD trajectory was run using the minimised structure as the starting conformation. The time step of the simulations was 2.0 fs with a cutoff of 10 Å for the nonbonded interaction, and SHAKE was employed to keep all bonds involving hydrogen atoms rigid. Constant-volume periodic boundary MD was carried out for 1.0 ns, during which the temperature was raised from 0 to 300 K. Then, 50 ns of constant-pressure periodic boundary MD was carried out at 300 K using the Langevin thermostat to maintain constant the temperature of our system.

All the α -carbons of the protein were blocked with a harmonic force constant of 10 kcal/mol Å². General Amber force field (GAFF) parameters were assigned to the ligand, while partial charges were calculated using the AM1-BCC method as implemented in the Antechamber suite of AMBER 14.

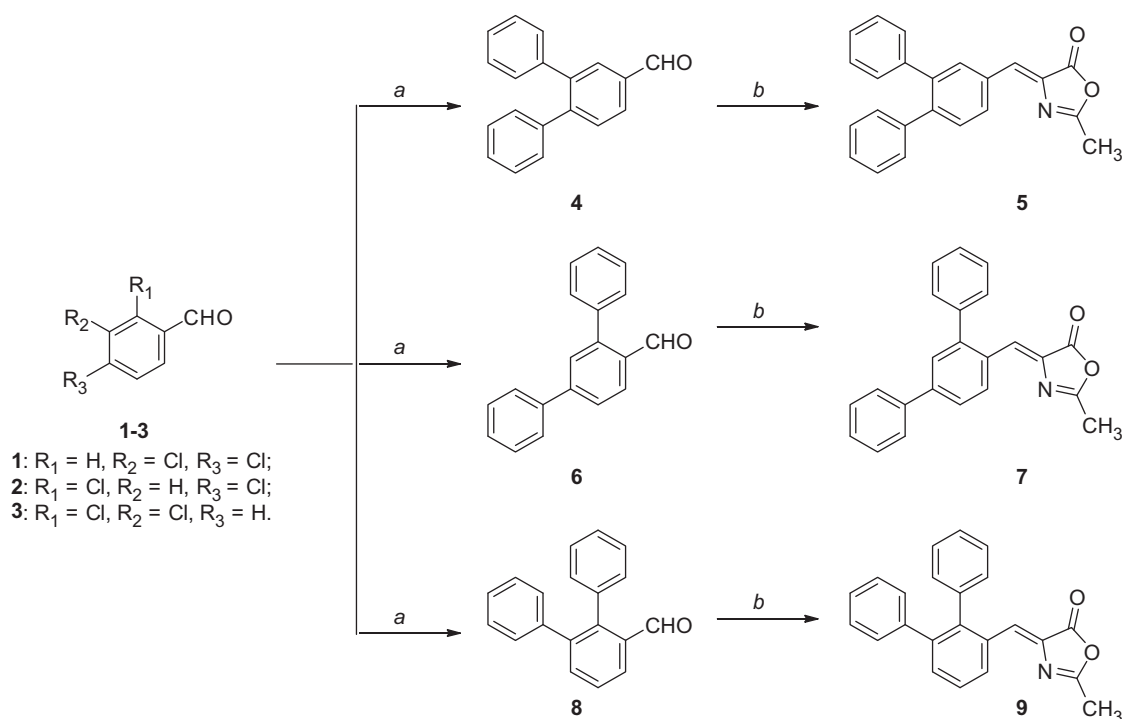
Binding energy evaluation

The evaluation of the binding energy associated to the two ligand–protein complexes analyzed through MD simulations was carried out using AMBER 14. The trajectories relative to the last 50 ns of each simulation were extracted and used for the calculation, for a total of 50 snapshots (at time intervals of 1 ns). Van der Waals, electrostatic and internal interactions were calculated with the SANDER module of AMBER 14, whereas polar energies were calculated using both the Generalised Born and the Poisson – Boltzman methods with the MM-PBSA module of AMBER 14. Dielectric constants of 1 and 80 were used to represent the gas and water phases, respectively, while the MOLSURF program was employed to estimate the nonpolar energies. The entropic term was considered as approximately constant in the comparison of the ligand – protein energetic interactions.

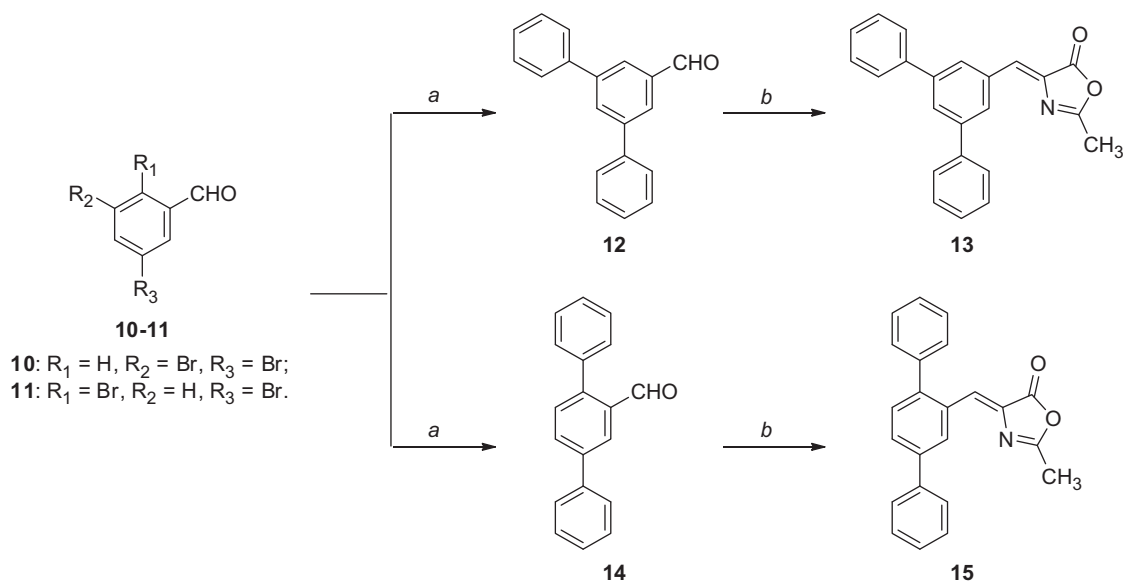
Results and discussion

Chemistry

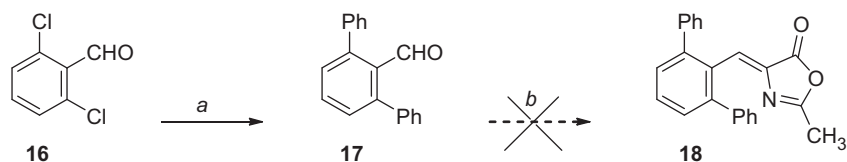
The terphenyl compounds were synthesised following the same synthetic strategy applied for the previous series of methyleneoxazol-5(4*H*)-one derivatives, differing only for the first step, in which a double cross-coupling reaction was necessary to replace both the halogen atoms by two phenyl rings in each appropriate dihalo-substituted precursor (Schemes 1 and 2). All the possible combinations of substitutions with phenyl rings in the central aromatic scaffold were explored, with the exception of the 2,6-diphenyl derivative (Scheme 3, see the following chapter for



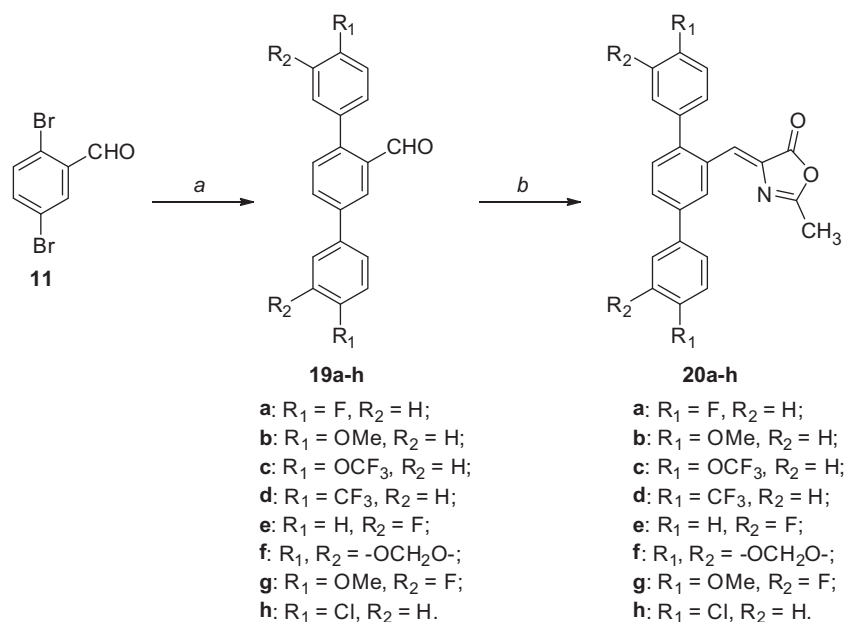
Scheme 1. Reagents and conditions: (a) for compound 4: phenylboronic acid, Pd(OAc)₂, K₃PO₄, TBAB, H₂O, 125 °C; for compound 6: phenylboronic acid, Pd(OAc)₂, PPh₃, aq. 2 M Na₂CO₃, toluene, EtOH, 100 °C; for compound 8: phenylboronic acid, Pd(OAc)₂, PPh₃, aq. 2 M Na₂CO₃, toluene, EtOH, 100 °C, then phenylboronic acid, Pd₂(dba)₃, Cs₂CO₃, Cy₃P 20% toluene, dioxane, 100 °C; (b) *N*-acetylglycine, Ac₂O, CH₃COONa, reflux.



Scheme 2. Reagents and conditions: (a) phenylboronic acid, Pd(OAc)₂, PPh₃, aq. 2 M Na₂CO₃, toluene, EtOH, 100 °C; (b) *N*-acetylglycine, Ac₂O, CH₃COONa, reflux.



Scheme 3. Reagents and conditions: (a) phenylboronic acid, Pd₂(dba)₃, Cs₂CO₃, Cy₃P 20% toluene, dioxane, 100 °C; (b) *N*-acetylglycine, Ac₂O, CH₃COONa, reflux.

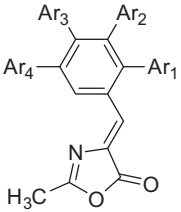


Scheme 4. Reagents and conditions: (a) variously substituted phenylboronic acid, Pd(OAc)₂, PPh₃, aq. 2 M Na₂CO₃, toluene, EtOH, 100 °C; (b) *N*-acetylglycine, Ac₂O, CH₃COONa, reflux.

discussion). According to the availability in our laboratory of the starting aldehydes, the coupling reactions were performed on dichloro- or dibromo-substituted compounds and different conditions were chosen on the basis of a preliminary prevision of the reaction outcome, which was highly dependent on the precursor structure. 3,4-Dichlorobenzaldehyde **1** was subjected to a Pd-catalyzed cross-coupling reaction under phosphine-free conditions in

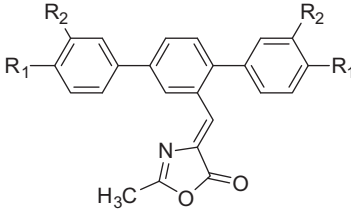
water, by using TBAB as the phase-transfer agent, in the presence of potassium phosphate, upon prolonged thermal heating⁴⁰, to give the diaryl derivative **4**. An Erlenmeyer-Plöchl condensation of the substituted aromatic aldehyde **4** with *N*-acetylglycine and sodium acetate in refluxing acetic anhydride gave the final product **5** as the (*Z*)-isomer (Scheme 1). In the case of 2,4-dichlorobenzaldehyde **2**, the classical thermal Pd(PPh₃)₄-catalyzed Suzuki

Table 1. Experimental inhibition activity (IC₅₀) on human MAGL and FAAH of the analyzed compounds.



5-13

#	Ar ₁	Ar ₂	Ar ₃	Ar ₄	MAGL IC ₅₀ (nM)	FAAH IC ₅₀ (nM)	MAGL/FAAH selectivity
5	H	Ph	Ph	H	837 ± 18	2321 ± 51	3
7	Ph	H	Ph	H	546 ± 20	18161 ± 904	33
9	Ph	Ph	H	H	2558 ± 172	20055 ± 1438	8
13	H	Ph	H	Ph	457 ± 10	14763 ± 1176	32
15	Ph	H	H	Ph	320 ± 10	10860 ± 161	34



15, 20a-h

#	R ₁	R ₂	MAGL IC ₅₀ (nM)	FAAH IC ₅₀ (nM)	MAGL/FAAH selectivity
20a	F	H	683 ± 50	27989 ± 1306	41
20b	OCH ₃	H	348 ± 38	36118 ± 1123	104
20c	OCF ₃	H	4194 ± 299	17728 ± 1198	4
20d	CF ₃	H	6763 ± 1125	28992 ± 1157	4
20e	H	F	628 ± 32	11713 ± 895	19
20f	-OCH ₂ O-	H	673 ± 23	23712 ± 1348	35
20g	OCH ₃	F	335 ± 2	22311 ± 1239	67
20h	Cl	H	476 ± 39	11487 ± 998	24
CAY10499			144 ± 4	14.7 ± 0.2	0.1
JZL-184			49.8 ± 4.2	3301 ± 205	66

conditions gave the desired product **6**. This may appear as a surprising outcome, because the starting material is an aryl chloride which generally is less reactive under these “mild” cross-coupling conditions that are commonly suitable for aryl bromides⁴¹. Nevertheless, the presence of the aldehyde group in *para* or *ortho*-position to the chloro atoms makes this compound more reactive toward the cross-coupling reaction (Scheme 1). Differently, in the case of 2,3-dichlorobenzaldehyde **3** we failed to perform the double cross-coupling by using simple Suzuki conditions, since ¹H-NMR analysis revealed the formation of only a mono-substitution product, probably due to the steric hindrance caused by the two chlorine atoms in adjacent positions to the aldehyde group. Therefore, the crude product of the reaction was subjected again to a second cycle of cross-coupling, adopting the Fu-type conditions⁴², which consists in using the more reactive catalytic system comprised of Pd₂(dba)₃, together with tricyclohexylphosphine as the catalyst ligand and cesium carbonate as the base (Scheme 1). Both compounds **6** and **8** were then transformed into the corresponding methyloxazol-5(4H)-one derivatives **7** and **9** as seen before for the preparation of **5** (Scheme 1).

The synthesis of terphenyl-methyloxazol-5(4H)-one compounds **13** and **15** started from bromo-aryl precursors **10** and **11** and cross-coupling, which were performed by adopting Suzuki conditions, allowed the formation of the diphenyl-substituted intermediates **12** and **14** with good yields, respectively (Scheme 2).

Finally, we tried to obtain the last derivative of this series of compounds, which derives from the combination of the two phenyl rings in both of the *ortho*-positions to the oxazolone ring (compound **18**, Scheme 3), starting from the 2,6-dichlorobenzaldehyde **16**. Unfortunately intermediate **17**, which was obtained in high yield from **16** by a Fu-type coupling, did not react under the classical Erlenmeyer-Plöchl conditions, neither by increasing the equivalents of the reagents (*N*-acetylglycine and acetic anhydride: two equivalents) or by extending the reaction time (24 or 48 h). This problem could be ascribed to the steric hindrance of the structure bearing two phenyl rings close to the aldehyde moiety, which hampered the formation of the additional five-membered cycle.

Considering the promising biological activity of compound **15** (see “Biological evaluation” section), which proved to be the most potent hMAGL inhibitor among all the possible combinations of terphenyl derivatives synthesised, a series of similar compounds variously substituted on the two peripheral aromatic rings were prepared, in order to investigate the effects of the additional substituents on the enzyme inhibition potency. All these compounds were obtained following the same synthetic pathway adopted for compound **15** (Scheme 2). 2,5-Dibromobenzaldehyde **11** was subjected to a double cross-coupling reaction using the Suzuki conditions with the appropriate boronic acid. Then, intermediates **19a-h** were reacted with *N*-acetylglycine and sodium acetate in

refluxing acetic anhydride to give the final compounds **20a–h** (Scheme 4).

Biological evaluation

The inhibitory effects of the newly synthesised compounds on human isoforms of MAGL and FAAH are reported in Table 1, together with those of reference inhibitors **CAY10499** and **JZL-184**.

Given the wide range of biological processes regulated by hydrolases, new MAGL inhibitors with a very high level of specificity should be required to minimise mechanism-based toxicities. Dual FAAH/MAGL inhibitors promote cataleptic and drug dependence behaviors in mice that are more reminiscent of direct CB1 agonists⁴³, underscoring the importance of maintaining high levels of selectivity to avoid simultaneous blockade of both FAAH and MAGL⁴⁴.

The series of diphenyl-substituted derivatives (**5**, **7**, **9**, **13**, and **15**) revealed that the presence of adjacent phenyl rings in the central scaffold is not ideal, since compound **5** (3,4-diphenyl) and, in particular, **9** (2,3-diphenyl), show the weakest potencies of this initial class. The introduction of further space between the two phenyl rings progressively improves the inhibition abilities of these compounds. In fact, when these substituents are placed in respective *meta*-positions (**7** and **13**), we can observe a significant improvement of the IC₅₀ values obtained. This effect is further enhanced when the two phenyl rings are placed in *para*-positions to each other, since compound **15** (2,5-diphenyl) displays the highest MAGL-inhibition potency (IC₅₀ = 320 nM) and MAGL/FAAH selectivity (34-fold) of this initial miniseries.

Therefore, we decided to further decorate the phenyl substituents of **15**, and extend the series of 2,5-diaryl-substituted methyleneoxazol-5(4*H*)-one derivatives (**20a–h**). The data reported in Table 1 show that relatively large substituents in the *para*-positions, such as OCF₃ (**20c**) and CF₃ (**20d**), do not seem to fit nicely in the enzyme active site since the MAGL-inhibitory activities associated to these compounds are very poor (IC₅₀ values of 4–6 μM). The introduction of small halogens, such as fluorine (**20a,e**) or chlorine (**20h**) atoms, or of a dioxolane portion (**20f**) is better tolerated, although the IC₅₀ values obtained with these compounds are always higher than that of **15**. Instead, the introduction of *para*-methoxy groups in the peripheral aryl rings, although they do not significantly improve the MAGL-inhibition potency of the resulting compounds (**20b**, **g**) when compared to their unsubstituted counterpart **15**, cause remarkable reductions of their FAAH-inhibitory abilities, thus resulting in a substantial increase in their MAGL/FAAH selectivity. This is particularly evident in **20b**: this compound displays an IC₅₀ values of 348 nM against MAGL (similar to that of **15**), together with a noticeable 104-fold selectivity for MAGL over FAAH, which is substantially higher than that shown by both its unsubstituted analog **15** and by reference inhibitor **JZL-184**. Comparing these results with those previously obtained for the monophenyl-substituted derivatives, we can highlight an improvement in terms of MAGL activity and MAGL/FAAH selectivity. In fact, the previously reported compounds showed a MAGL activity in the low micromolar range (IC₅₀ = 1.0–2.2 μM) and a MAGL/FAAH selectivity from 15 up to 69-fold¹⁸. Conversely, the most active compounds of this series (**15**, **20b**, **20g**) displayed IC₅₀ values ranging from 320 to 348 nM, thus the presence of two phenyl rings placed in *para*-positions to each other markedly increased the inhibitory potency on MAGL. Moreover, the presence of a methoxy group in *para*-position on both phenyl rings allowed an increase in the MAGL/FAAH selectivity up to 104-fold, as for

compound **20b**. Therefore, this compound can be considered as the most promising inhibitor of the present series of methyleneoxazol-5(4*H*)-one derivatives.

In order to study the inhibition mechanism of the new reported compounds, the effects of preincubation and dilution in the inhibitory ability of compound **20b** were evaluated. In the preincubation experiments, an irreversible inhibitor will increase its capacity to block the enzyme with increasingly longer incubation times in the presence of enzyme prior to addition of substrate; a constant IC₅₀, conversely, supports a reversible mechanism⁴⁵. As expected, compound **20b** did not show any significant increase in its ability to block MAGL activity after 30 and 60 min (Figure 3(A)), supporting that it should be a reversible inhibitor. In the dilution experiments, if **20b** is an irreversible inhibitor, then its inhibition potency should not drop upon dilution, whereas inhibition levels should be substantially reduced upon dilution in presence of a reversible compound. As shown in Figure 3(B), **20b** showed reversible inhibition, since the inhibition produced by 10 μM of the compound is significantly higher compared with the inhibition observed upon 40× dilution, which appears similar to that produced by a 0.25 μM concentration of the compound.

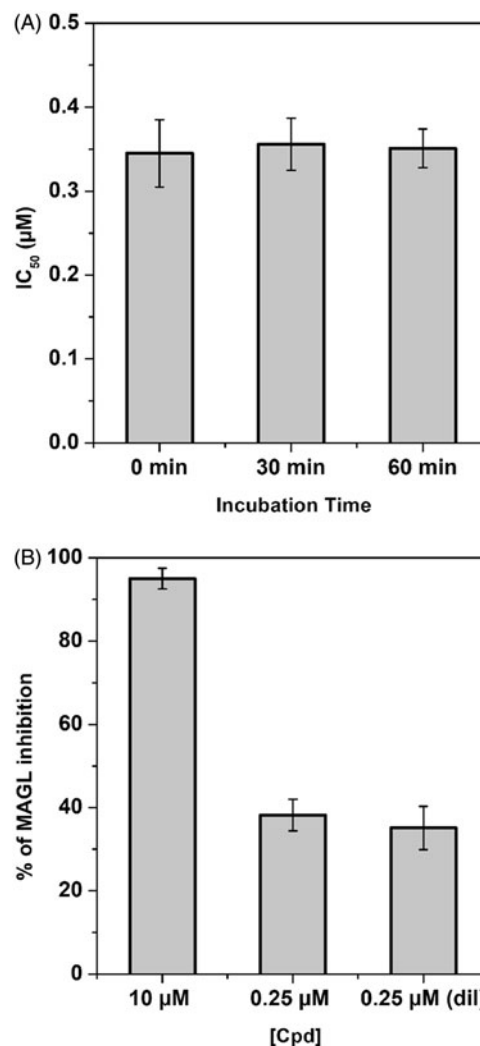


Figure 3. Compound **20b**-MAGL inhibition analysis. (A) IC₅₀ (μM) values of **20b** at different preincubation times with *h*MAGL (0, 30 and 60 min). (B) Dilution assay: the first two columns indicate the inhibition percentage of compound **20b** at a concentration of 10 and 0.25 μM. The third column indicates the inhibition percentage of compound **20b** after dilution (final concentration = 0.25 μM).

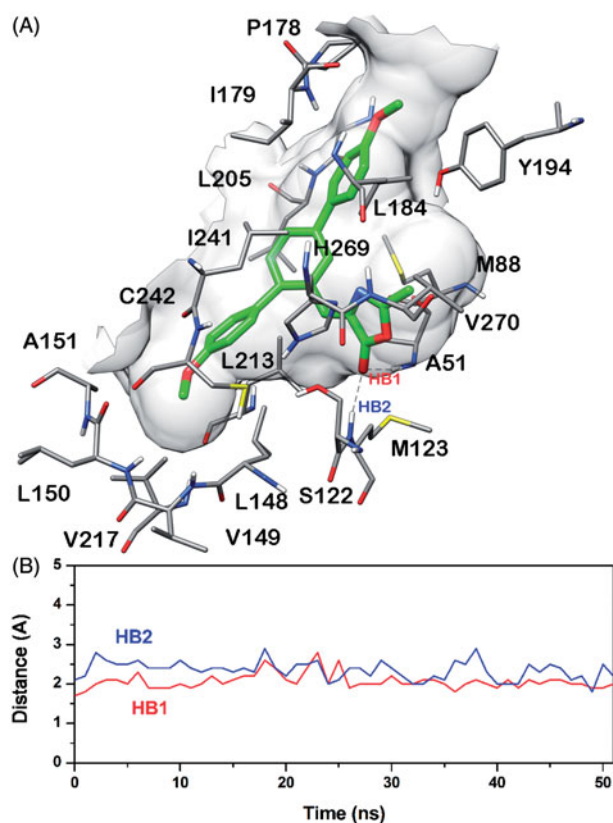


Figure 4. Minimised average structure of compound **20b** docked into MAGL receptor (A) and analysis of **20b**-MAGL H-bond interactions (B). The plot shows the distance analysis for the two H-bonds (i.e. HB1 and HB2).

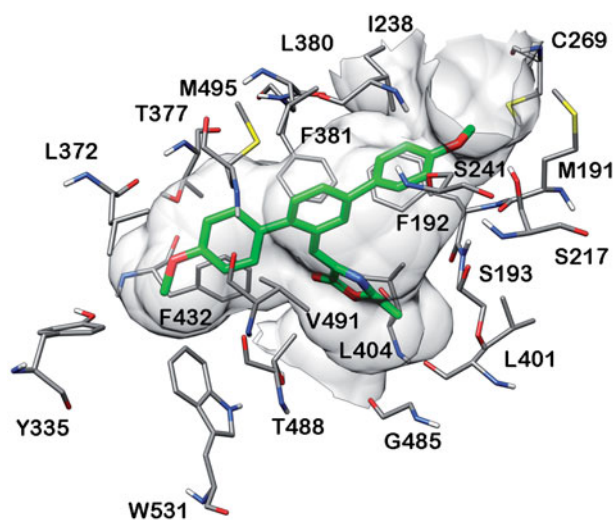


Figure 5. Minimised average structure of compound **20b** docked into FAAH receptor.

Compounds **20b** was also selected for *in vitro* experiments to evaluate its antiproliferative potency on cancer cells. Two human ovarian cancer cell lines, OVCAR3 and CAOV3, were chosen because western blot analysis highlighted an overexpression of MAGL in these two cell lines¹⁷. The compound produced appreciable inhibition of cell viability for both cell lines, with IC_{50} values of 41.6 μ M for OVCAR3 and 23.8 μ M for CAOV3. Furthermore, it showed negligible potency against noncancerous human mesenchymal stem cells (*hMSC*, IC_{50} > 100 μ M).

Table 2. MM-PBSA results for compound **20b** docked into MAGL and FAAH.

Protein	Ele	VdW	PBSur	PB	Δ PBSA
MAGL	-12.5	-52.2	43.4	-5.2	-26.5
FAAH	-3.2	-50.1	40.2	-5.3	-18.5

Δ PBSA is the sum of the electrostatic (Ele), van derWaals (VdW), polar (PB) and non-polar (PBSur) solvation free energy. Data are expressed as $\text{kcal}\cdot\text{mol}^{-1}$.

Molecular modeling studies

To suggest a possible binding mode for this class of derivatives, the interaction of compound **20b** with MAGL and FAAH was analyzed by means of docking and MD simulations. This docking analysis helps us to identify the most significant interactions of the compound before the formation of the covalent bond with the catalytic serine, thus highlighting the key points for the ligand recognition. As a first step, a consensus docking method was applied as it is shown to predict the ligand-binding pose better than the single docking programs⁴⁶. By using this kind of approach, one ligand is docked into the target protein by means of different docking procedures. Then, among the different best-ranked poses (originated by the different docking procedures) the pose in common with the largest number of docking procedures is considered as the best docking pose. The **20b**-MAGL and **20b**-FAAH complexes obtained by means of this docking strategy were then subjected to 51 ns of MD simulation with explicit water molecules, as described in the "Material and methods" section. Figure 4(A) shows the main interactions of **20b** with MAGL. The dimethoxyterphenyl fragment occupies the central core of the binding site showing a large number of lipophilic interactions such as those with L148, A151, P178, I179, L184, L205, L213 and L241; whereas the 2-methyloxazolone ring is placed near the catalytic S122 and forms two H-bonds with the nitrogen backbone of A51 (HB1, Figure 4(A)) and M123 (HB2, Figure 4(A)). Interestingly, as shown in Figure 4(B) the H-bonds interactions between the ligand and A51 and M123 displayed a high stability, as they were maintained for the whole MD simulation.

As shown in Figure 5, the binding site shape of FAAH does not seem to allow an interaction of the 2-methyloxazolone ring of **20b** in proximity to the catalytic region of the enzyme. The ligand shows a binding disposition that is completely different from that observed in the MAGL binding site, and the 2-methyloxazolone ring is ~ 10 Å away from the catalytic S241. Furthermore, the compound does not form any H-bonds with the protein and the ligand is stabilised only by lipophilic interactions with F192, I238, L380, L404 and F432.

In order to further analyze the interaction of **20b** into MAGL and FAAH, the two MD trajectories were further analyzed through the MM-PBSA method⁴⁷, which has shown to accurately estimate the ligand-protein energy interaction⁴⁸⁻⁵⁰. This approach averages contributions of gas-phase energies, solvation free energies, and solute entropies calculated for snapshots of the complex molecule as well as the unbound components extracted from MD trajectories, according to the procedure fully described in "Material and methods" section. The MM-PBSA results (Table 2) suggested that the interaction of **20b** with the MAGL binding cavity was more stable by ~ 8 kcal/mol than its interaction with FAAH and this energy difference was mainly determined by the lack of strong electrostatic interactions into the FAAH-binding site.

Conclusions

In summary, we designed and synthesised a new class of terphenyl-2-methyloxazol-5(4*H*)-one derivatives by optimising the benzylidene-2-methyloxazol-5(4*H*)-one scaffold, which was

previously identified as a suitable moiety able to efficiently interact with the MAGL-binding site. The reported structural optimisation led to the identification of compound **20b**, which displayed a high MAGL-inhibition activity with an IC₅₀ value of 348 nM together with a very good MAGL/FAAH selectivity ratio. Moreover, the biochemical experiments confirmed the reversible properties of this compound and, finally, cell-based assays showed promising cell growth inhibitory activities in the OVCAR-3 and CAOV3 cell lines which overexpress MAGL. Since the *in vivo* possible application of reversible MAGL inhibitors has only recently been explored, mainly due to the deficiency of known compounds possessing efficient reversible inhibitory activities, the present findings constitute an interesting extension to the knowledge of the MAGL inhibition.

Disclosure statement

No potential conflict of interest was reported by the authors.

Funding

The authors would like to extend their sincere appreciation to the University of Pisa for its funding on this research through the project no. PRA_2017_51.

ORCID

Carlotta Granchi  <http://orcid.org/0000-0002-5849-0722>
 Filippo Minutolo  <http://orcid.org/0000-0002-3312-104X>
 Tiziano Tuccinardi  <http://orcid.org/0000-0002-6205-4069>

References

- Di Marzo V, Petrosino S. Endocannabinoids and the regulation of their levels in health and disease. *Curr Opin Lipidol* 2007;18:129–40.
- Labar G, Wouters J, Lambert DM. A review on the monoacylglycerol lipase: at the interface between fat and endocannabinoid signalling. *Curr Med Chem* 2010;17:2588–607.
- Mulvihill MM, Nomura DK. Therapeutic potential of monoacylglycerol lipase inhibitors. *Life Sci* 2013;92:492–7.
- Nomura DK, Morrison BE, Blankman JL, et al. Endocannabinoid hydrolysis generates brain prostaglandins that promote neuroinflammation. *Science* 2011;334:809–13.
- Kinsey SG, O'Neal ST, Long JZ, et al. Inhibition of endocannabinoid catabolic enzymes elicits anxiolytic-like effects in the marble burying assay. *Pharmacol Biochem Behav* 2011;98:21–7.
- Ramesh D, Ross GR, Schlosburg JE, et al. Blockade of endocannabinoid hydrolytic enzymes attenuates precipitated opioid withdrawal symptoms in mice. *J Pharmacol Exp Ther* 2011;339:173–85.
- Kopp F, Komatsu T, Nomura DK, et al. The glycerophospho metabolome and its influence on amino acid homeostasis revealed by brain metabolomics of GDE1(-/-) mice. *Chem Biol* 2010;17:831–40.
- Muccioli GG, Labar G, Lambert DM. CAY10499, a novel monoglyceride lipase inhibitor evidenced by an expeditious MGL assay. *Chembiochem* 2008;9:2704–10.
- Zvonok N, Pandarinathan L, Williams J, et al. Covalent inhibitors of human monoacylglycerol lipase: ligand-assisted characterization of the catalytic site by mass spectrometry and mutational analysis. *Chem Biol* 2008;15:854–62.
- King AR, Lodola A, Carmi C, et al. A critical cysteine residue in monoacylglycerol lipase is targeted by a new class of isothiazolinone-based enzyme inhibitors. *Br J Pharmacol* 2009;157:974–83.
- Long JZ, Li W, Booker L, et al. Selective blockade of 2-arachidonoylglycerol hydrolysis produces cannabinoid behavioral effects. *Nat Chem Biol* 2009;5:37–44.
- Matuszak N, Muccioli GG, Labar G, Lambert DM. Synthesis and *in vitro* evaluation of N-substituted maleimide derivatives as selective monoglyceride lipase inhibitors. *J Med Chem* 2009;52:7410–20.
- Kapanda CN, Masquelier J, Labar G, et al. Synthesis and pharmacological evaluation of 2,4-dinitroaryldithiocarbamate derivatives as novel monoacylglycerol lipase inhibitors. *J Med Chem* 2012;55:5774–83.
- Schlosburg JE, Blankman JL, Long JZ, et al. Chronic monoacylglycerol lipase blockade causes functional antagonism of the endocannabinoid system. *Nat Neurosci* 2010;13:1113–19.
- Hernandez-Torres G, Cipriano M, Heden E, et al. A reversible and selective inhibitor of monoacylglycerol lipase ameliorates multiple sclerosis. *Angew Chem Int Ed Engl* 2014;53:13765–70.
- Tuccinardi T, Granchi C, Rizzolio F, et al. Identification and characterization of a new reversible MAGL inhibitor. *Bioorg Med Chem* 2014;22:3285–91.
- Granchi C, Rizzolio F, Palazzolo S, et al. Structural optimization of 4-chlorobenzoylpiperidine derivatives for the development of potent, reversible, and selective monoacylglycerol lipase (MAGL) inhibitors. *J Med Chem* 2016;59:10299–314.
- Granchi C, Rizzolio F, Bordoni V, et al. 4-Arylidene-2-methoxyazolo-5(4H)-one as a new scaffold for selective reversible MAGL inhibitors. *J Enzyme Inhib Med Chem* 2016;31:137–46.
- Poli G, Giuntini N, Martinelli A, Tuccinardi T. Application of a FLAP-consensus docking mixed strategy for the identification of new fatty acid amide hydrolase inhibitors. *J Chem Inf Model* 2015;55:667–75.
- Maestro, version 9.0. Portland (OR): Schrödinger Inc; 2009. Available from: <https://www.schrodinger.com/>
- MacroModel, version 9.7. Portland (OR): Schrödinger Inc; 2009. Available from: <https://www.schrodinger.com/>
- Poli G, Martinelli A, Tuccinardi T. Reliability analysis and optimization of the consensus docking approach for the development of virtual screening studies. *J Enzym Inhib Med Ch* 2016;31:167–73.
- Bertrand T, Auge F, Houtmann J, et al. Structural basis for human monoglyceride lipase inhibition. *J Mol Biol* 2010;396:663–73.
- Mileni M, Kamtekar S, Wood DC, et al. Crystal structure of fatty acid amide hydrolase bound to the carbamate inhibitor URB597: discovery of a deacylating water molecule and insight into enzyme inactivation. *J Mol Biol* 2010;400:743–54.
- Sanner MF. Python: a programming language for software integration and development. *J Mol Graph Model* 1999;17:57–61.
- Morris GM, Huey R, Lindstrom W, et al. AutoDock4 and AutoDockTools4: automated docking with selective receptor flexibility. *J Comput Chem* 2009;30:2785–91.
- DOCK, version 6.5. San Francisco (CA): Molecular Design Institute, University of California; 1998. Available from: <http://dock.compbio.ucsf.edu/>
- QUACPAC, version 1.5.0. Santa Fe (NM): OpenEye Scientific Software, Inc.; 2013. Available from: <https://www.eyesopen.com/>

29. FRED, version 3.0.0. Santa Fe (NM): OpenEye Scientific Software, Inc.; 2013. Available from: <https://www.eyesopen.com/>
30. OMEGA, version 2.4.6. Santa Fe (NM): OpenEye Scientific Software, Inc.; 2013. Available from: <https://www.eyesopen.com/>
31. Hawkins PC, Skillman AG, Warren GL, et al. Conformer generation with OMEGA: algorithm and validation using high quality structures from the Protein Databank and Cambridge Structural Database. *J Chem Inf Model* 2010;50:572–84.
32. Hawkins PC, Nicholls A. Conformer generation with OMEGA: learning from the data set and the analysis of failures. *J Chem Inf Model* 2012;52:2919–36.
33. Tuccinardi T, Poli G, Dell'Agnello M, et al. Receptor-based virtual screening evaluation for the identification of estrogen receptor beta ligands. *J Enzym Inhib Med Ch* 2015;30:662–70.
34. Glide, version 5.0. Portland (OR): Schrödinger Inc; 2009.
35. Verdonk ML, Cole JC, Hartshorn MJ, et al. Improved protein-ligand docking using GOLD. *Proteins* 2003;52:609–23.
36. Trott O, Olson AJ. AutoDock Vina: improving the speed and accuracy of docking with a new scoring function, efficient optimization, and multithreading. *J Comput Chem* 2010;31:455–61.
37. Korb O, Monecke P, Hessler G, et al. pharmACophore: multiple flexible ligand alignment based on ant colony optimization. *J Chem Inf Model* 2010;50:1669–81.
38. Case DA, Berryman JT, Betz RM, et al. AMBER, version 14. San Francisco (CA): University of California; 2015.
39. York DM, Darden TA, Pedersen LG. The effect of long-range electrostatic interactions in simulations of macromolecular crystals - a comparison of the ewald and truncated list methods. *J Chem Phys* 1993;99:8345–8.
40. Leadbeater NE, Marco M. Ligand-free palladium catalysis of the Suzuki reaction in water using microwave heating. *Org Lett* 2002;4:2973–6.
41. Miyaura N, Suzuki A. Palladium-catalyzed cross-coupling reactions of organoboron compounds. *Chem Rev* 1995;95:2457–83.
42. Littke AF, Fu GC. A convenient and general method for Pd-catalyzed Suzuki cross-couplings of aryl chlorides and arylboronic acids. *Angew Chem Int Edit* 1998;37:3387–8.
43. Long JZ, Nomura DK, Vann RE, et al. Dual blockade of FAAH and MAGL identifies behavioral processes regulated by endocannabinoid crosstalk in vivo. *Proc Natl Acad Sci USA* 2009;106:20270–5.
44. Chang JW, Niphakis MJ, Lum KM, et al. Highly selective inhibitors of monoacylglycerol lipase bearing a reactive group that is bioisosteric with endocannabinoid substrates. *Chem Biol* 2012;19:579–88.
45. Wang X, Sarris K, Kage K, et al. Synthesis and evaluation of benzothiazole-based analogues as novel, potent, and selective fatty acid amide hydrolase inhibitors. *J Med Chem* 2009;52:170–80.
46. Tuccinardi T, Poli G, Romboli V, et al. Extensive consensus docking evaluation for ligand pose prediction and virtual screening studies. *J Chem Inf Model* 2014;54:2980–6.
47. Kuhn B, Kollman PA. Binding of a diverse set of ligands to avidin and streptavidin: an accurate quantitative prediction of their relative affinities by a combination of molecular mechanics and continuum solvent models. *J Med Chem* 2000;43:3786–91.
48. Tuccinardi T, Manetti F, Schenone S, et al. Construction and validation of a RET TK catalytic domain by homology modeling. *J Chem Inf Model* 2007;47:644–55.
49. Tuccinardi T, Granchi C, Iegre J, et al. Oxime-based inhibitors of glucose transporter 1 displaying antiproliferative effects in cancer cells. *Bioorg Med Chem Lett* 2013;23:6923–7.
50. Petrou A, Geronikaki A, Terzi E, et al. Inhibition of carbonic anhydrase isoforms I, II, IX and XII with secondary sulfonamides incorporating benzothiazole scaffolds. *J Enzym Inhib Med Ch* 2016;31:1306–11.